

Ride Comfort Enhancement of Semi-active Vehicle Suspension Based on SMC with PID Sliding Surface Parameters Tuning using PSO

Ahmed O. Bashir, Xiaoting Rui, Laith K. Abbas, Jianshu Zhang

*Institute of Launch Dynamics, Nanjing University of Science and Technology,
Nanjing 210094, P R China, (e-mail: mecheng5120@yahoo.com, ruixt@163.net (Corresponding author),
laithabbass@yahoo.com, zhangjs_nust@sina.com).*

Abstract: This paper presents a sliding mode control (SMC) using proportional-integral-differential (PID) sliding surface (SMC-PID) for semi-active vehicle suspension system utilizing magneto-rheological (MR) fluid damper to enhance ride comfort. The fundamental concept is that the robustness property of SMC and good response traits of PID are incorporated to accomplish more acceptable overall performance. The sliding surface design is modified based on PID and is derived from the developed dynamic equations. A dynamical model for five-degrees of freedom half car committing MR damper is developed. The particle swarm optimization (PSO) technique is applied to solve the nonlinear system optimization problem to find the PID sliding surface controller parameters. Optimal setting of these parameters will improve dynamic response and ensure stability of the system. Capability of the proposed controller has been evaluated by numerical simulations. Comparisons with MR-Passive and conventional SMC system have also been provided. From the observation of the simulation results, compared to the MR-Passive system and conventional SMC controlled system, the SMC-PID controlled system can offer a better ride comfort at adapting bump and random road excitations.

Keywords: 5DOF vehicle semi-active suspension, MR-damper, SMC-PID control Ride comfort.

1. INTRODUCTION

With the advances in the controllable damper manufacturing, the semi-active shock absorbers are finding their way as crucial devices for vibration suppression, particularly in automotive suspension systems. This is assigned to the concept that the damping coefficients in semi-active systems can be adapted to improve ride comfort and road handling performances. The task of the vast majority of these systems relies on Magneto-Rheological (MR) dampers due to their potential use as semi-active control devices (Kelso, 2001; Dyke et al., 1996). The significance and attracting characteristics of these devices come from their capability to dynamically vary their properties to solid state by varying the magnetic field; furthermore, they require a minimal amount of power for activation of the fluid. However, the outcomes of uncertainties and nonlinearities are usually facing by the MR damper system, which simultaneously yields incredible difficulties in the development of the control system employed in the MR damper system. Unsatisfied system performance will be seen if inappropriate control scheme is applied.

In the past decades, different classes of control approaches have been performed for applications of MR dampers in semi-active suspension systems related to ride comfort and vehicle stability. (Batterbee and Sims, 2007) conducted experimental work using the hardware-in-the-loop simulation method (HWLSM) to investigate the controller performance, where the controller is tested in MR shock absorber committed with semi-active suspension system (SASS).

(Sung and Choi, 2011) proposed a cylindrical type MR shock absorber using a quarter vehicle MR electronic control suspension to improve ride comfort and driving stability. Simulation work was conducted for investigation of a full-vehicle MR system. (Yu et al., 2009) incorporated a human simulated intelligent control (HSIC) scheme in the half-car exerting MR suspension system model. The vibration control response of semi-active suspension system for pitch angle acceleration was assessed via computer simulation. (Unger et al., 2013) performed a test work utilizing a semi-active full-car model based on linear quadratic (LQ) controller. The optimization of controller was done to accomplish enhanced ride comfort and decrease in the braking distance. The test outcomes indicated enhanced performance of LQ controller in semi-active vehicle to fulfil targeted objectives compared to passive and skyhook-based controllers. (Paksoy et al., 2014) arranged fuzzy logic and self-tuning fuzzy logic controller (S-FLC) for vibration attenuation in a semi-active full vehicle model with seven degrees of freedom. Simulation results demonstrated that the effectiveness of (S-FLC) is the best contrasted with uncontrolled and Fuzzy Logic controlled suspension systems. (Rajagopal and Ponnusamy, 2014) utilized Bio-geography-Based Optimization of PID controller to decrease the Vibration levels of Active Suspension System (ASS). (Prabakar et al., 2009) proposed an optimal preview control of four degrees of freedom semi-active vehicle model utilizing MR damper under random road excitation. (Rossi and Lucente, 2004) utilized H-infinity control strategy (HICS) to quarter car and half-car semi-active suspension systems in order to enhance the ride comfort and road handling performance. (Eltantawie, 2012) developed a decentralized

neuro-fuzzy controller to improve the ride and stability of the half-car model with the MR damper. They have evaluated the performance of the half-car model under two different road conditions (road bump and random road undulations) as inputs. They have also compared the obtained results with the passive suspension system (PSS). (Karkoub and Zribi, 2006) used analytical method to assess the effectiveness of the MR damper in vibration reduction by using a half-car model based on optimal control scheme. The drawbacks of such strategies lie in the nature of their tuning and the inability to address robustness guarantees.

On the other hand, numerous methods have been proposed against the existing issues, particularly addressed to the development of the robust control system to overcome the system parameters variation, uncertainties and disturbances. A wise and proper control approach will be needed in dealing with the complexity and the challenges in the control of the MR damped system. Sliding mode control is widely used in various applications that exposes to the disturbances and the system parameters variation (Edwards and Spurgeon, 1998). The reason for the popular use of the SMC is the robustness of the modelling errors as well as its insensitivity to the parameter variations and extraneous disturbances (Kaya, 2007; Rossi and Lucente, 2004). Nevertheless, in practical usages, chattering is the disadvantage of a solely design of SMC, which is a high-frequency variation of the control input due to the pre-existence of system un-modelled dynamics. Chattering should be avoided because, it has destructive impact for the mechanical part of systems, and also it may lead to instability.

Different sliding mode control methods have been stated for the usages of MR dampers in semi-active suspension systems related to vehicle ride comfort and stability, whereas, they barely accomplished appropriate performance. (Choi et al., 2003) performed a sliding mode controller (SMC) to suppress the vibration of Electro-Rheological (ER) damped semi-active seat suspension system. (Yao et al., 2013) employed sliding mode control system to control a semi-active MR suspension and approved the performance of this strategy by means of hardware-in-loop simulation. (Rajkumar et al., 2015) stated fuzzy based sliding mode controller for vibration reduction of quarter-car incorporated seat suspension with driver model. (Zhang et al., 2015) proposed a sliding mode controller for semi-active vehicle suspension employing magneto-rheological damper. (Chen et al., 2011) designed a SMC method for semi-active suspension systems (SASS), and this is a full-state feedback control. But it seems difficult to measure or estimate some of the state information, such as tire deflection or road disturbance. (Bashir et al., 2018) proposed an intelligent proportional-integral-differential sliding mode control (i-PIDSMC) to improve ride quality of MR damped vehicle suspension system. However, in his work PID controller parameters were tuned according to Ziegler-Nichols method. It is recognized from the previous research work that, the development of more efficient control algorithm for MR damped vehicle suspension system to improve performance with strong robustness is a hard issue.

In this context, tuning the PID sliding surface gains of sliding mode control (SMC) with proportional-integral-differential sliding surface (SMCPID) based on particle swarm optimization (PSO) is proposed. The main target of the proposed controller is to get better performance for MR-damped half vehicle suspension system. The novelty of this paper is rather limited. The primary contribution lies in the extension of the application of the SMC with PID Sliding Surface tuned by using PSO to the control of a 5DOF half vehicle semi-active suspension system by utilizing MR-damper as the actuator. Simulation results shows its feasibility.

In the conventional sliding mode, the sliding mode gain is determined solely by the desired closed loop poles. Therefore, the sliding surface is completely reliant on the sliding mode gain. In the SMCPID, the sliding surface gain is determined by the desired closed loop gain and the design parameter that can be adjusted to fulfil the sliding surface requirement. The sliding surface design is modified based on PID and same is derived from the developed dynamics equations, and MR damped half-car integrating with seat suspension model is demonstrated. The stability of the control system is proved using Lyapunov theorem. Subsequently, the model is examined on road bump and random profile. The performance of the proposed approach is compared with conventional SMC controlled system as reported in (Yuvapriya et al., 2018), and MR-passive suspension system.

This paper is organized as below. Section 2 gives a brief explanation of the MR damped vehicle suspension system. The SMCPID algorithm is presented and explained in Section 3. The simulation results are presented and discussed in Section 4. Finally, conclusions are provided in Section 5.

2. DESCRIPTION OF THE MODEL

2.1 Half car dynamic model

A 5DOF half vehicle active suspension system is well documented in the literature for control applications (El-taweel and Metered, 2018; Demir et al., 2012). In this section, a half-car model(HCM) having MR shock absorber assembled in primary suspension system is presented as shown in Fig. 1. The complete model represents a real system with adopted parameters as the driver seat mass, sprung as well as the front and rear un-sprung masses (m_3, m_2, m_{1f}, m_{1r}); I denotes vehicle moment of inertia; primary front and rear spring stiffness (k_{2f}, k_{2r}); front and rear tyre stiffness (k_{1f}, k_{1r}); seat spring stiffness and damping coefficient(k_3, c_3); seat displacement, front and rear sprung mass displacements, front and rear un-sprung mass displacement ($z_3, z_{2f}, z_{2r}, z_{1f}, z_{1r}$) whereas z_{0f} and z_{0r} represents road input displacement for front and rear respectively. z_2 is the vertical displacement at the gravity centre of vehicle body and θ is the body angular

displacement in pitch direction. a , b and e denote the horizontal distances from the centre of gravity of the vehicle body to the front, rear wheel axles and the position of seat, respectively. P_s is the chassis vertical displacement passing through the seat mass centre. In case of semi-active behaviour of suspension system, MR shock absorber is liable for generation of extra controllable damping forces f_{MRf} and f_{MRr} .

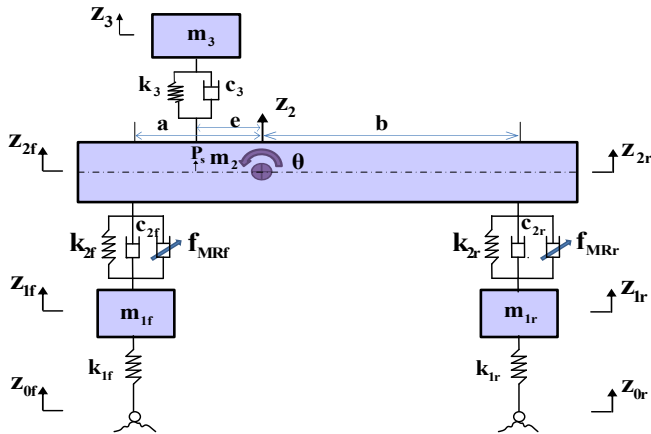


Fig. 1. Half-car model with 5DOF.

By considering only, the vertical and pitch motions of complete structure, the governing dynamical equations of the five degree-of-freedom system can be presented as follows:

$$\begin{cases} p_s = z_2 - e\theta \\ z_{2f} = z_2 - a\theta \\ z_{2r} = z_2 + b\theta \end{cases} \quad (1)$$

$$m_2 \ddot{z}_2 = -k_{2f}(z_{2f} - z_{1f}) - c_{2f}(\dot{z}_{2f} - \dot{z}_{1f}) - k_{2r}(z_{2r} - z_{1r}) - c_{2r}(\dot{z}_{2r} - \dot{z}_{1r}) + k_3(z_3 - z_{ps}) + c_3(\dot{z}_3 - \dot{z}_{ps}) + f_{MRf} + f_{MRr} \quad (2)$$

$$I \ddot{\theta} = \{k_{2f}(z_{2f} - z_{1f}) + c_{2f}(\dot{z}_{2f} - \dot{z}_{1f})\}a - \{k_{2r}(z_{2r} - z_{1r}) + c_{2r}(\dot{z}_{2r} - \dot{z}_{1r})\}b + \{k_3(z_3 - z_{ps}) + c_3(\dot{z}_3 - \dot{z}_{ps})\}e - af_{MRf} + bf_{MRr} \quad (3)$$

$$m_3 \ddot{z}_3 = k_3(z_3 - z_{ps}) + c_3(\dot{z}_3 - \dot{z}_{ps}) \quad (4)$$

$$m_{1f} \ddot{z}_{1f} = k_{2f}(z_{2f} - z_{1f}) + c_{2f}(\dot{z}_{2f} - \dot{z}_{1f}) - k_{1f}(z_{1f} - z_{0f}) - f_{MRf} \quad (5)$$

$$m_{1r} \ddot{z}_{1r} = k_{2r}(z_{2r} - z_{1r}) + c_{2r}(\dot{z}_{2r} - \dot{z}_{1r}) - k_{1r}(z_{1r} - z_{0r}) - f_{MRr} \quad (6)$$

State variables for state space representation can be defined as:

$$x_1 = z_{1f}, \quad x_2 = \dot{z}_{1f}, \quad x_3 = z_{1r}, \quad x_4 = \dot{z}_{1r}, \quad x_5 = z_2,$$

$$x_6 = \dot{z}_2, \quad x_7 = z_3, \quad x_8 = \dot{z}_3, \quad x_9 = \theta, \quad x_{10} = \dot{\theta}$$

The mathematical equations of half car system (2-6) can be revised in the state-space form as:

$$\begin{aligned} \dot{X}(t) &= AX(t) + BU(t) + DW(t) \\ Y(t) &= CX(t) \end{aligned} \quad (7)$$

where;

$$X = [x_1 \ x_2 \ x_3 \ x_4 \ x_5 \ x_6 \ x_7 \ x_8 \ x_9 \ x_{10}]^T$$

$$A = \begin{bmatrix} 0 & 1 & 0 & 0 & 0 & 0 & 0 & 0 & 0 & 0 \\ \frac{-a}{m_f} & \frac{-c_{2f}}{m_f} & 0 & 0 & \frac{k_{2f}}{m_f} & \frac{c_{2f}}{m_f} & 0 & 0 & \frac{ak_{2f}}{m_f} & \frac{ac_{2f}}{m_f} \\ 0 & 0 & 0 & 1 & 0 & 0 & 0 & 0 & 0 & 0 \\ 0 & 0 & \frac{-a}{m_r} & \frac{-c_{2r}}{m_r} & \frac{k_{2r}}{m_r} & \frac{c_{2r}}{m_r} & 0 & 0 & \frac{bk_{2r}}{m_r} & \frac{bc_{2r}}{m_r} \\ 0 & 0 & 0 & 0 & 0 & 1 & 0 & 0 & 0 & 0 \\ \frac{k_{2f}}{m_2} & \frac{c_{2f}}{m_2} & \frac{k_{2r}}{m_2} & \frac{c_{2r}}{m_2} & \frac{\omega_3}{m_2} & \frac{\omega_4}{m_2} & \frac{k_3}{m_2} & \frac{c_3}{m_2} & \frac{\omega_5}{m_2} & \frac{\omega_6}{m_2} \\ 0 & 0 & 0 & 0 & 0 & 0 & 0 & 1 & 0 & 0 \\ 0 & 0 & 0 & 0 & \frac{k_3}{m_3} & \frac{c_3}{m_3} & \frac{k_3}{m_3} & \frac{c_3}{m_3} & \frac{ek_3}{m_3} & \frac{ec_3}{m_3} \\ 0 & 0 & 0 & 0 & 0 & 0 & 0 & 0 & 0 & 1 \\ \frac{ak_{2f}}{I} & \frac{ac_{2f}}{I} & \frac{bk_{2r}}{I} & \frac{bc_{2r}}{I} & \frac{\omega_7}{I} & \frac{\omega_8}{I} & \frac{ek_3}{I} & \frac{ec_3}{I} & \frac{\omega_9}{I} & \frac{\omega_{10}}{I} \end{bmatrix}$$

$$B = \begin{bmatrix} 0 & \frac{1}{m_f} & 0 & 0 & 0 & \frac{1}{m_2} & 0 & 0 & 0 & \frac{a}{I} \\ 0 & 0 & 0 & \frac{1}{m_r} & 0 & \frac{1}{m_2} & 0 & 0 & 0 & \frac{b}{I} \end{bmatrix}, \quad U(t) = [f_{MRf} \quad f_{MRr}]^T$$

$$D = \begin{bmatrix} 0 & \frac{k_{1f}}{m_{1f}} & 0 & 0 & 0 & 0 & 0 & 0 & 0 & 0 \\ 0 & 0 & 0 & \frac{k_{1r}}{m_{1r}} & 0 & 0 & 0 & 0 & 0 & 0 \end{bmatrix}, \quad W(t) = [z_{0f} \quad z_{0r}]^T$$

$$\text{and } C = \begin{bmatrix} 1 & 0 & 0 & 0 & 0 & 0 & 0 & 0 & 0 & 0 \\ 0 & 0 & 1 & 0 & 0 & 0 & 0 & 0 & 0 & 0 \\ 0 & 0 & 0 & 0 & 0 & 1 & 0 & 0 & 0 & 0 \\ 0 & 0 & 0 & 0 & 0 & 0 & 0 & 0 & 0 & 1 \end{bmatrix}$$

$$\begin{aligned} \omega_1 &= k_{1f} + k_{2f}, \quad \omega_2 = k_{1r} + k_{2r}, \quad \omega_3 = k_3 + k_{2f} + k_{2r}, \\ \omega_4 &= c_3 + c_{2f} + c_{2r}, \quad \omega_5 = ek_3 + ak_{2f} - bk_{2r}, \quad \omega_6 = ec_3 + ac_{2f} - bc_{2r}, \\ \omega_7 &= -ek_3 + ak_{2f} - bk_{2r}, \quad \omega_8 = -ec_3 + ac_{2f} - bc_{2r}, \\ \omega_9 &= a^2k_{2f} - e^2k_3 + b^2k_{2r} \text{ and } \omega_{10} = a^2c_{2f} - e^2c_3 + b^2c_{2r} \end{aligned}$$

2.2 MR-damper model

The half-car is suspended with an MR damper. The damper model is selected as in (Spencer Jr et al., 1997) and the structure of the model is shown in Fig.2. The theoretical characteristics of the MR damper at various control voltages are shown in Fig.3. The applied voltage range is from 0 to 2.0V with an increment of 0.5V. The displayed features for

the sinusoidal excitation frequency of 1.92Hz and the excitation amplitude of 25mm are obtained. The MR damper shows a wide range controllable dynamic under magnetic field and the theoretical predictions are used to design the half-car semi-active suspension applying MR dampers.

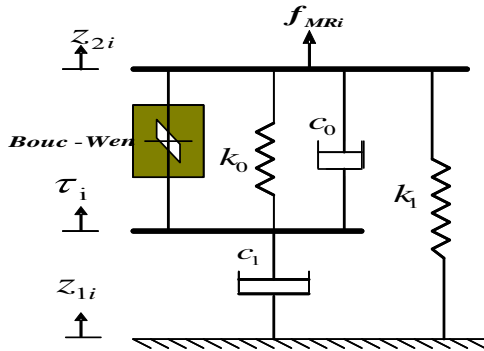


Fig. 2. MR-damper model.

MR damper has been placed between sprung and un-sprung masses in parallel to the passive suspension. By using Newton's second law, one can derive the force predicted by this model as follows:

$$f_{MRi} = \alpha z + k_0(z_{2i} - \tau_i) + c_0(\dot{z}_{2i} - \dot{\tau}_i) + k_1(z_{2i} - z_{1i}) \quad (8)$$

$$(z_{2i} - \tau_i) = \frac{1}{c_0 + c_1} \{-\alpha z + k_0(z_{2i} - \tau_i) + c_0(\dot{z}_{2i} - \dot{\tau}_i)\} \quad (9)$$

The displacement z is defined as

$$\dot{z} = -\gamma \cdot (|\dot{z}_{2i} - \dot{\tau}_i|) \cdot z \cdot |z|^{n-1} + (\dot{z}_{2i} - \dot{\tau}_i) \cdot (\delta - \beta |z|^n) \quad (10)$$

The total force f_{MRi} provided by the device is obtained by

$$f_{MRi} = -c_1(z_{2i} - \tau_i) + k_1((z_{2i} - z_{1i}) - x_0) \quad (11)$$

The subscript i refers to the chassis frontal and rear. The adaptation of hysteresis parameters α , β and δ finds out the linearity in the unloading region besides transition smoothness from the pre-yield to the post-yield region. The parameters γ , β , δ , n and k_1 are regarded constant; x_0 is the preliminary deflection of the gas spring accumulator and the parameters c_0 , c_1 and α , are assumed to be functions of the voltage signal u .

$$\left. \begin{aligned} \alpha &= \alpha(u) = \alpha_a + \alpha_b u \\ c_1 &= c_1(u) = c_{1a} + c_{1b} u \\ c_0 &= c_0(u) = c_{0a} + c_{0b} u \end{aligned} \right\} \quad (12)$$

$$\dot{u} = -\eta(u - v) \quad (13)$$

k_1 is represents the accumulator stiffness; c_1 , k_0 are the viscous damping and stiffness at higher velocities, respectively; η is the time constant, α is the yield-pressure parameter describing the MR fluid and v is the command

voltage dispatched to the current driver. Table 1 depicts the parameter values of the model.

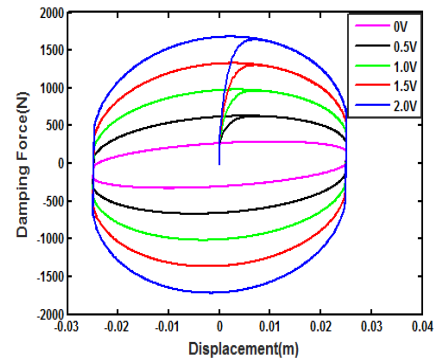


Fig. 3. Characteristics of the MR damper.

Table 1. Parameters of the damper model (Lai and Liao, 2002)

Symbol	Value (Unit)	Symbol	Value (Unit)
C_{0a}	784 N.s/m	α_a	12441 N/m
C_{0b}	1803 N.s/Vm	α_b	38430 N/Vm
K_0	3610 N/m	γ	136320 m ⁻²
C_{1a}	14649 N.s/m	β	2059020 m ⁻²
C_{1b}	34622 N.s/Vm	δ	58
K_1	840 N/m	n	2
x_0	0.0245 m	η	190 s ⁻¹

From the above modelling process, the key purpose of the control issue is to adjust the input voltage of MR damper according to vehicle body motions and external road disturbances and further to acquire the changeable damping force, thus can enhance the ride quality.

3. CONTROL ALGORITHM

In general, semi-active control through MR damper is accomplished by two levels of control, the damper controller and the system controller. The damper controller is utilized to create and modify the command voltage and to track the desired damping force that the system controller specifies based on the desired and actual damping force (Wang and Liao, 2005). Equations (8-13) have to be used to estimate actual damping force and implemented along with equations (1-7). A brief description is provided in the following subsections.

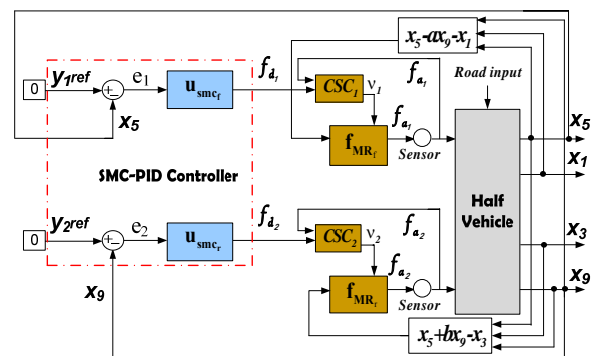


Fig. 4. Structure of the control system.

3.1 System Controller

Unlike the damper control, the system controller is responsible for creating the desired damping force in accordance with the plant's dynamic behaviour. It is necessary to use appropriate and simple control policy to realize reasonable performance under various road excitation. The suggested control scheme used in this study is a sliding mode control (SMC) using proportional-integral-derivative (PID) sliding surface as shown in Fig. 4.

3.1.1 Sliding mode controller design

The control signal in SMC design comprises of equivalent control and switching control as explained in equation (14). The equivalent control, u_{eq} stands for the sliding phase when $s(t) = 0$ (Kaya, 2007, Eker, 2006). While the switching control u_{sw} stands for the reaching phase when $s(t) \neq 0$.

$$u_{smc}(t) = u_{eq}(t) + u_{sw}(t) \quad (14)$$

To design SMC, since the suspension system is a second order system, the sliding surface is chosen as,

$$s = y_2 + \lambda y_1 \quad (15)$$

where λ is the sliding surface gain. By differentiation

$$\dot{s} = \dot{y}_2 + \lambda \dot{y}_1 \quad (16)$$

The system moves on the sliding mode at $\dot{s} = 0$

$$0 = \dot{y}_2 + \lambda \dot{y}_1 \quad (17)$$

Two MR dampers are mounted between the sprung and unsprung masses of the vehicle frontal and rear suspension. To design the control force u_{smc_f} of the front wheel, let the state variables y_1 and y_2 represent suspension working space of the front wheel, and car body velocity, respectively. From the geometrical and state variables for state space, the front suspension working space is

$$y_1 = (x_5 - ax_9) - x_1 \quad (18)$$

and the front car velocity is

$$y_2 = (\dot{x}_5 - a\dot{x}_9) \quad (19)$$

Substituting equations (18) and (19) into (17), yields

$$u_{smc_f} = k_{2f}((x_5 - ax_9) - x_1) + c_{2f}((x_6 - ax_{10}) - x_2) + k_{2r}((x_5 + bx_9) - x_3) + c_{2r}((x_6 + bx_{10}) - x_4) + k_3((x_5 - ex_9) - x_7) + c_3((x_6 - ex_{10}) - x_8) - m_2\lambda((x_6 - ax_{10}) - x_2) + m_2a\dot{x}_{10} - f_{MRr} - k_1 \text{sign}_1(s_1) \quad (20)$$

Similarly, for the rear suspension working space

$$y_1 = (x_5 + bx_9) - x_3 \quad (21)$$

and the car velocity of the rear wheel is

$$y_2 = (\dot{x}_5 + b\dot{x}_9) \quad (22)$$

By substituting equations (21) and (22) into (17), the rear control force can be obtained as

$$u_{smc_r} = k_{2f}((x_5 - ax_9) - x_1) + c_{2f}((x_6 - ax_{10}) - x_2) + k_{2r}((x_5 + bx_9) - x_3) + c_{2r}((x_6 + bx_{10}) - x_4) + k_3((x_5 - ex_9) - x_7) + c_3((x_6 - ex_{10}) - x_8) - m_2\lambda((x_6 - ax_{10}) - x_2) - m_2b\dot{x}_{10} - f_{MRf} - k_2 \text{sign}_2(s_2) \quad (23)$$

where $k_1 \text{sign}_1(s)$ and $k_2 \text{sign}_2(s)$ are the switching functions, and k_1, k_2 are positive constants, which meets the desired criteria $\dot{s}s < 0$ and brings the system into the sliding surface then merges to zero.

3.1.2 Sliding mode controller design using PID sliding surface

Construction of the sliding surface is the most important step in the design of the SMC, which is expected to meet the desired control requirements and performance. The trajectories of the states are forced to reach and remain on the sliding surface. In this study, we utilized the PID sliding surface in the SMC design as follows:

$$s_1 = k_{11}e_1 + k_{12}\dot{e}_1 + k_{13}\int_0^t e_1 dt \quad (24)$$

$$s_2 = k_{21}e_2 + k_{22}\dot{e}_2 + k_{23}\int_0^t e_2 dt$$

where; k_{ij} is the PID design parameter (Ghazali et al., 2011), which is chosen in a manner to make system asymptotically stable. Let the tracking error of the vertical and the angular displacements be

$$e_1 = x_5 - y_{1ref} \quad (25)$$

$$e_2 = x_9 - y_{2ref}$$

where; y_{1ref} , and y_{2ref} are desired states. Now from (24) the differential of sliding surface (\dot{s}):

$$\dot{s}_1 = k_{11}\dot{e}_1 + k_{12}\ddot{e}_1 + k_{13}e_1 \quad (26)$$

$$\dot{s}_2 = k_{21}\dot{e}_2 + k_{22}\ddot{e}_2 + k_{23}e_2$$

Substituting the values of tracking error from (25), and equations (1) and (2) into equation (26) one can obtain:

$$\dot{s}_1 = k_{12}\left\{\frac{k_{11}}{k_{12}}(x_6 - \dot{y}_{1ref}) + \frac{k_{13}}{k_{12}}(x_5 - y_{1ref}) + \Psi_1 + \ddot{y}_{1ref} + \frac{u_s}{m_2}\right\} \quad (27)$$

$$\dot{s}_2 = k_{22}\left\{\frac{k_{21}}{k_{22}}(x_{10} - \dot{y}_{2ref}) + \frac{k_{23}}{k_{22}}(x_9 - y_{2ref}) + \Psi_2 + \ddot{y}_{2ref} + \frac{u_\phi}{I}\right\}$$

where;

$$\Psi_1 = m_2^{-1} \begin{pmatrix} -k_{2f}((x_5 - ax_9) - x_1) - c_{2f}((x_6 - ax_{10}) - x_2) - \\ k_{2r}((x_5 + bx_9) - x_3) - c_{2r}((x_6 + bx_{10}) - x_4) - \\ k_3((x_5 - ex_9) - x_7) - c_3((x_6 - ex_{10}) - x_8) + \\ f_{MRf} + f_{MRr} \end{pmatrix}$$

$$\Psi_2 = I^{-1} \begin{pmatrix} (k_{2f}((x_5 - ax_9) - x_1) + c_{2f}((x_6 - ax_{10}) - x_2))a - \\ (k_{2r}((x_5 + bx_9) - x_3) + c_{2r}((x_6 + bx_{10}) - x_4))b - \\ (k_3((x_5 - ex_9) - x_7) + c_3((x_6 - ex_{10}) - x_8))e - \\ af_{MRf} + bf_{MRr} \end{pmatrix}$$

u_{eq} is calculated from (27) by putting $\dot{s}_1, \dot{s}_2 = 0$, and one can obtain:

$$u_{z_{eq}} = -m_2 k_{12} \left(\frac{k_{11}}{k_{12}} (x_6 - \dot{y}_{1ref}) + \frac{k_{13}}{k_{12}} (x_5 - y_{1ref}) + \Psi_1 + \ddot{y}_{1ref} \right) \quad (28)$$

$$u_{\varphi_{eq}} = -I k_{22} \left(\frac{k_{21}}{k_{22}} (x_{10} - \dot{y}_{2ref}) + \frac{k_{23}}{k_{22}} (x_9 - y_{2ref}) + \Psi_2 + \ddot{y}_{2ref} \right)$$

The switching control can be chosen as a sign function of sliding surface (Ghazali et al., 2011), hence the following switching control law is proposed:

$$u_{z_{\sigma}} = -\eta_1 s_1 \text{sign}(s_1) \quad (29)$$

$$u_{\varphi_{\sigma}} = -\eta_2 s_2 \text{sign}(s_2)$$

where, $\eta_1 > 0$ and $\eta_2 > 0$ stands for the discontinuous gain. It should be noted that the implementation of the control input described in (29) results in a very high switching frequency which in turn causes undesired chattering (Komurcugil and Biricik, 2017). Therefore, the chattering is reduced by employing saturation function (Mu, 2010) as follows:

$$u_{z_{\sigma}} = -\eta_1 s_1 \text{sat}(s_1, \varepsilon) \quad (30)$$

$$u_{\varphi_{\sigma}} = -\eta_2 s_2 \text{sat}(s_2, \varepsilon)$$

where;

$$\text{sat}(s_1, \varepsilon) = \text{sat}(s_2, \varepsilon) = \begin{cases} 1 & , s > \varepsilon \\ s/\varepsilon, \|s\| \leq \varepsilon \text{ and } \varepsilon > 0. \\ -1 & , s < -\varepsilon \end{cases}$$

From (28) and (30) the controller equation is given by:

$$u_z = u_{z_{eq}} + u_{z_{\sigma}} = -\ddot{e}_1 - \frac{k_{11}}{k_{12}} \dot{e}_1 - \frac{k_{13}}{k_{12}} e_1 - \eta_1 s_1 \text{sat}(s_1, \varepsilon)$$

$$u_{\varphi} = u_{\varphi_{eq}} + u_{\varphi_{\sigma}} = -\ddot{e}_2 - \frac{k_{21}}{k_{22}} \dot{e}_2 - \frac{k_{23}}{k_{22}} e_2 - \eta_2 s_2 \text{sat}(s_2, \varepsilon) \quad (31)$$

3.1.3 Proof of Stability

To verify the stability behaviour of the controller, two Lyapunov functions are introduced which define stability for two sliding surfaces s_1 and s_2 in the form of:

$$V_1 = \frac{1}{2} s_1^2 \quad (32)$$

$$V_2 = \frac{1}{2} s_2^2$$

with $V(0) = 0$ and $V(t) > 0$ for $s \neq 0$

To guarantee the trajectory move from reaching phase to sliding phase and ensure the stability, it is necessary to follow the reaching condition:

$$\dot{V}(t) < 0 \text{ for } s \neq 0 \quad (33)$$

From (32), derivative of the Lyapunov function is defined as:

$$\dot{V}_1 = s_1 \dot{s}_1 \quad (34)$$

$$\dot{V}_2 = s_2 \dot{s}_2$$

Substituting (27) into (34)

$$\dot{V}_1 = s_1 \left(k_{12} \left(\frac{k_{11}}{k_{12}} (x_6 - \dot{y}_{1ref}) + \frac{k_{13}}{k_{12}} (x_5 - y_{1ref}) + \Psi_1 + y_{1ref} + \frac{u_z}{m_2} \right) \right) \quad (35)$$

$$\dot{V}_2 = s_2 \left(k_{22} \left(\frac{k_{21}}{k_{22}} (x_{10} - \dot{y}_{2ref}) + \frac{k_{23}}{k_{22}} (x_9 - y_{2ref}) + \Psi_2 + y_{2ref} + \frac{u_{\varphi}}{I} \right) \right)$$

Putting values in (31) into (34) and (35):

$$\dot{V}_1 = s_1 (-\eta_1 s_1 \text{sat}(s_1, \varepsilon)) \quad (36)$$

$$\dot{V}_2 = s_2 (-\eta_2 s_2 \text{sat}(s_2, \varepsilon))$$

To prove the reaching condition, (36) finally becomes:

$$\dot{V}_1 < -\eta_1 (|s_1|)^2 \quad \text{for } s \neq 0 \quad (37)$$

$$\dot{V}_2 < -\eta_2 (|s_2|)^2$$

The parameters that guarantee the stability are η_1 and η_2 which makes the function \dot{V} , negative definite function when $\eta_1 > 0, \eta_2 > 0$, hence on the basis of equation (37) it can be easily inferred that above design follows Lyapunov stability theory.

3.2 Damper controller

There are different types of MR damper controllers, and this study will focus on continuous-state control. The continuous-state control was employed by (Metered et al., 2010) and (Lam and Liao, 2003) to calculate the voltage signal applied to the MR Damper's coil, by a simple feedback control strategy that the response of the MR damper could be linearized. Indicating the values of the voltage to the current

driver associated within saturation of the MR damper by V_{\max} , the minimum voltage to the damper (i.e.0V) by V_{\min} , the required control force determined by the system controller and the damping force of MR damper are f_d and f_a , respectively. The input voltage is expressed as

$$v_i = \begin{cases} V_{\max}, & \xi > V_{\max} \\ V_{\min}, & \xi < V_{\min} \\ \xi, & \text{Otherwise} \end{cases} \quad (38)$$

where;

$$\xi = G(f_{d_i} - Hf_{a_i}) \text{sgn}(f_{a_i}) \quad i = (1,2) \text{ refer to}$$

front and rear, respectively. The values of G , H and V_{\max} were set to be $0.0038V/N$, 1 and $2V$ respectively, as in (Lam and Liao, 2003).

3.3 Optimization of PID sliding surface gains using PSO

The ride quality is related to vehicle acceleration. Therefore, the absolute value of the maximum body vertical acceleration (BVA) and front suspension working space (FSWS) are chosen as the objective function that could be minimized through PSO algorithm. The nonlinear optimization problem which determines the controller gains k_{ij} is described by equation (39).

$$\text{Minimize } J(k) = \left(\frac{1}{T} \int_0^T (\|\ddot{z}_2\|^2 + \|FSWS\|^2) dt \right)^{1/2} \quad (39)$$

where T is the total time period.

The PSO algorithm is a computational strategy which optimizes a predefined problem by iteratively attempting to improve a candidate solution regarding a given measure of quality. Firstly, PSO algorithm searches about the optimum solution by initializing some random particles in the solution space. Each particle is interacted with two sets of factors, namely the velocity and position.

The velocity and position of the particles are updated based on the equations (40) and (41) respectively (Eberhart and Kennedy, 1995).

$$v_p^{j+1} = wv_p^j + c_1r_1(b_p^j - y_p^j) + c_2r_2(g_p^j - y_p^j) \quad (40)$$

$$y_p^{j+1} = y_p^j + v_p^{j+1} \quad (41)$$

where; y_p^j and y_p^{j+1} are the current and future searching point, v_p^j and v_p^{j+1} denotes the current and future velocities, while b_p^j and g_p^j are the velocities based upon the personal best and global best respectively, r_1 and r_2 are randomly generated numbers in between 0 and 1, and w is inertia weight parameter. The values of c_1 and c_2 are acceleration

constant set to constant value 2. The above mentioned optimization stages are summarized in Fig 5.

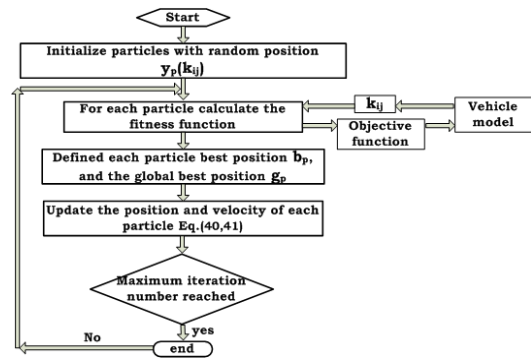


Fig. 5. Steps in PSO algorithm.

4. NUMERICAL SIMULATION AND RESULTS

To evaluate the ride comfort of the half car model (HCM), the body vertical acceleration (BVA), front suspension working space (FSWS) and seat displacement (SD) are considered as essential performance criteria that manage the ride comfort. SMC-PID is designed and compared with SMC and MR-Passive. We consider a half-car model shown in Fig 1, which is excited to demonstrate the control performance of the proposed controller by two types of road inputs, such as bump input (BI) and random input (RI). The model parameters are shown in Table (2). as in (Demir et al., 2012). The simulations are performed in MATLAB/SIMULINK toolbox which enables the modelling and dynamic simulation of the control system. For the bump and random inputs, the front and rear wheel have delay time of $(a+b)/v_s$.

Type 1: Bump road excitation

The bump road profile shown in Fig. 6 is used. The bump profile is mathematically described by (Choi and Kim, 2000) as

$$z_r(t) = \begin{cases} a_m(1 - \cos(\omega_r(t - 0.5))), & \text{for } 0.5 \leq t \leq 0.5 + d_b/v_s \\ 0, & \text{otherwise} \end{cases} \quad (42)$$

where; a_m is the half of bump amplitude, $\omega_r = 2\pi v_s/d_b$, d_b is the bump width, v_s is the bump velocity and z_r is the road excitation. The parameter values of; a_m, d_b and v_s are $0.03m$, $10m$ and $20m/s$ respectively.

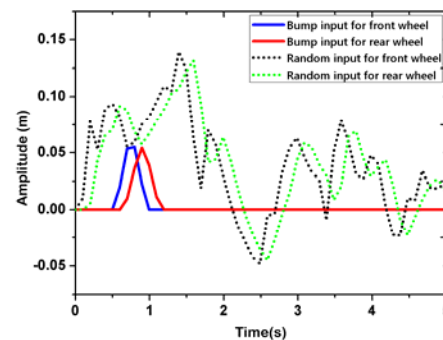


Fig. 6. Road profiles.

Table 2. Half vehicle model parameters

Symbol	Value (Unit)	Symbol	Value (Unit)
m_{1f}	38kg	c_{2f}	960N.s/m
m_{1r}	38kg	c_{2r}	960N.s/m
m_2	550kg	c_3	1620N.s/m
I	2100kg.m ²	k_{1f}	160KN/m
m_3	80kg	k_{1r}	160KN/m
k_{2f}	16KN/m	a	1.2m
k_{2r}	16KN/m	b	1.5m
k_3	5KN/m	e	0.4m

The time responses of FSWS, BVA and SD for SMC-PID, SMC and MR-Passive with BI are shown in Figs.7 (a- c) and the peak to peak (PTP) values are presented in Tables.4 (a-c). The amplitude and oscillation are increased and the vibration is slowly reduced with MR-Passive.

The oscillation of SD, FSWS and BVA for HCM is increased and it settles after 3.5seconds with MR-Passive. The peak to peak values of SD, FSWS and BVA are reached to 0.0782 m 0.05475 m and 2.918m/s², respectively. Therefore, peak to peak, oscillation and settling time have a significant impact on the vehicle's riding quality. To enhance the travelling comfort of the vehicle, SMC-PID is designed for HCM with semi-active suspension system.

Referring to Tables.4 (a-c) the peak to peak values of SD, FSWS and BVA with SMC reaches 0.0747m, 0.04234m and 2.503m/s², respectively. Similarly, the peak to peak values of FSWS, BVA and SD with SMC-PID reaches 0.02126m, 1.859m/s² and 0.06914m, respectively. The overall steady state performance for HCM under BI may be achieved with SMC-PID. The results of the time responses show that the SMC-PID works better than the SMC and the MR-Passive.

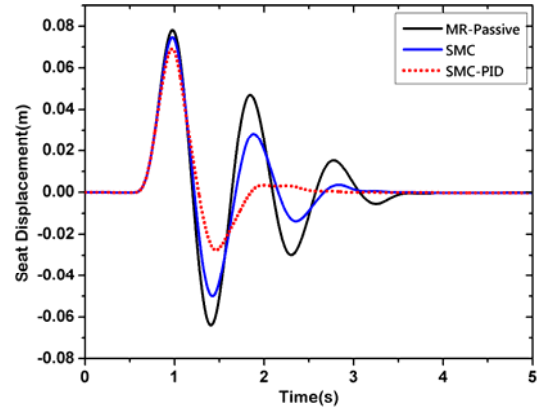
The following parameters are initialized for PSO:

- Population size : 15
- Number of variables to be tuned : 6
- Initial population : Random selection
- Maximum inertia weight : 0.9
- Number of iterations : 10
- Weight factors (c_1, c_2) : 2, 2

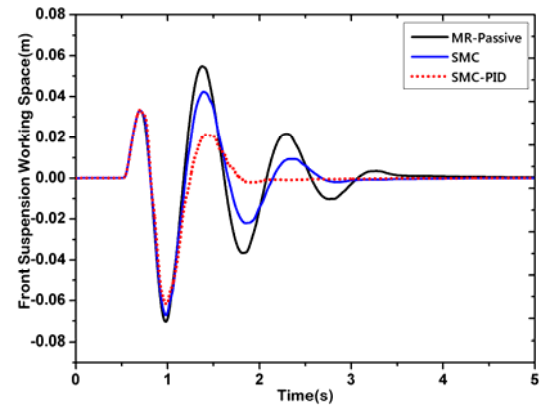
The optimization problem given in equation (39) has been solved employing the above initialized parameters, together with values of decision variable (K_{ij}) shown in Table 3. For the fitness function value evolution during the optimization process, the PSO algorithm converges to the optimal parameters after 10 iterations. The computed optimal parameters are: $K_{11}=31$; $K_{12}=15.2$; $K_{13}=29$; $K_{21}=52.4867$; $K_{22}=1.05$ and $K_{23}=5$. The converging characteristic of PSO technique for SMC-PID controller parameters is shown in Fig. 8.

The control force of front suspension for bump road input shown in Fig. 9, guarantees the better system performance. The SMC-PID controller takes the control effort necessary to suppress the vibration of BI when compared to SMC. In the

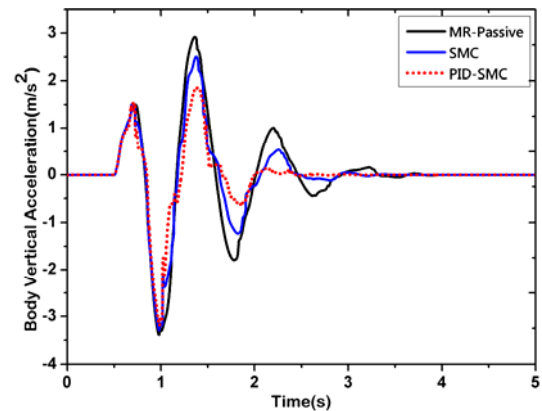
meantime, an input control voltage comparison for the MR damper is provided in Fig.10. The input control voltage controlled by SMC-PID controller is relatively large because its suspension deflection is smaller than that of SMC and MR-Passive suspension. The results of the simulation show again the validity of the SMC-PID controller. The percentage improvements of the peak to peak values of FSWS, BVA and SD using SMC-PID, SMC and MR-Passive are shown in Tables. 4(a-c). The PTP values of FSWS, BVA and SD are greatly reduced and the riding quality is improved with SMC-PID compared to SMC and MR-Passive suspension system.



(a)



(b)



(c)

Fig. 7. The time response of the system under excitation of road bump. (a) SD, (b) FSWS and (c) BVA.

Table 3. Range of the controller tuning parameters

Parameter	K_{11}	K_{12}	K_{13}	K_{21}	K_{22}	K_{23}
Minimum	1	1	1	1	1	1
Maximum	50	30	50	100	10	40

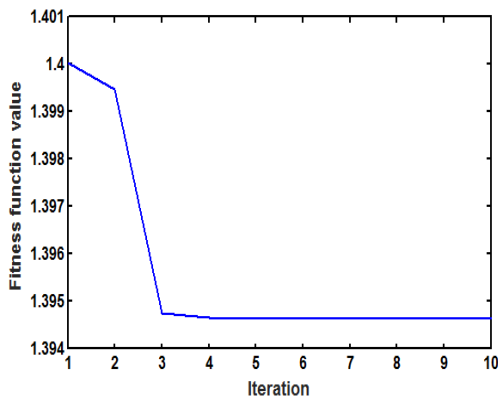


Fig. 8. The convergence characteristic of PSO-SMC-PID.

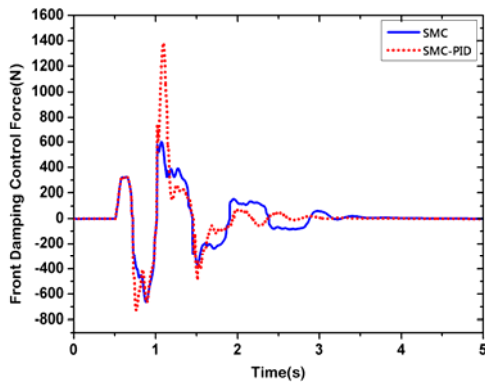


Fig. 9. The control force of front wheel for BI.

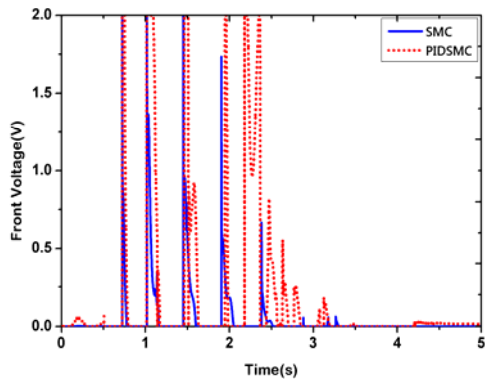


Fig. 10. Input control voltage for MR-damper.

Table 4(a). The PTP values of SD for BI.

System Type	SD (m)	% Reduction Respect to MR-Passive	% Reduction Respect to SMC
MR-Passive	0.0782	---	---
SMC	0.0747	4.48	---
SMC-PID	0.06914	11.59	7.44

Table 4(b). The PTP values of FSWS for BI

System Type	FSWS (m)	% Reduction Respect to MR-Passive	% Reduction Respect to SMC
MR-Passive	0.05475	---	---
SMC	0.04234	22.67	---
SMC-PID	0.02126	61.17	49.79

Table 4(c). The PTP of values of BVA for BI

System Type	BVA (m/s ²)	% Reduction Respect to MR-Passive	% Reduction Respect to SMC
MR-Passive	2.918	---	---
SMC	2.503	14.22	---
SMC-PID	1.859	36.29	25.73

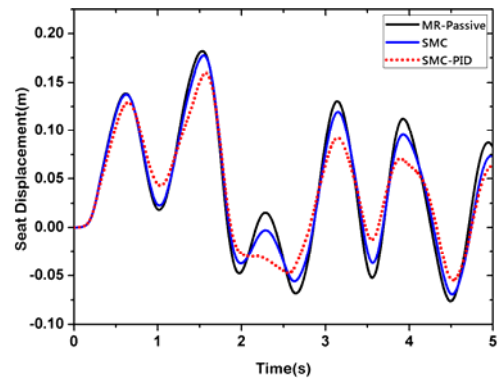
Type 2: Random road excitation

The road random excitation model shown in Fig. 6 is built by using integrated Gaussian white noise. The equation of random road in time domain can be expressed as (Hu et al., 2017).

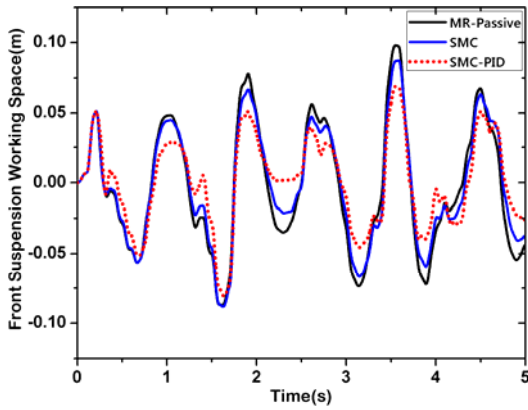
$$\dot{z}_r(t) = -\alpha_s \cdot v_s \cdot z_r(t) + \delta_s \sqrt{G_q(n_0)} \cdot v_s \cdot w_0(t) \quad (43)$$

where; $z_r(t)$ is road roughness amplitude, $w_0(t)$ is a white noise whose intensity is 1, $v_s = 20\text{m/s}$ is vehicle speed, $G_q(n_0)$ is road roughness coefficient which is constant and decided by road conditions. Class D road profile was selected in this work to be the main road profile. For road of D level, $G_q(n_0) = 1024e-6\text{m}^3$ and the values of coefficients α_s and δ_s are 0.06283m^{-1} and 0.6283m respectively.

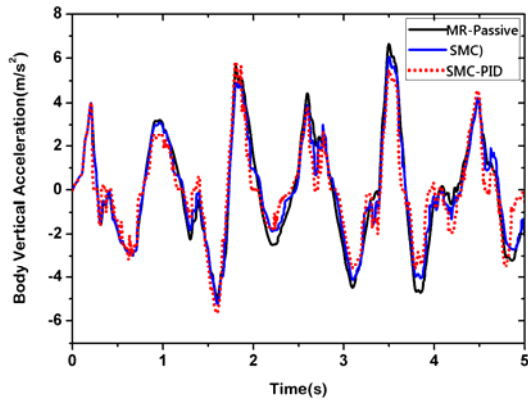
For the MR-Passive, SMC controlled and SMC-PID controlled suspension system the time histories of SD, FSWS and BVA under random road input are presented in Figs.11 (a-c), respectively. The root mean square (RMS) values of HCM semi-active suspension system controlled by SMC-PID compared with SMC controlled and MR-Passive suspension system are provided in Fig.12. Here, the road surface is non-uniform and the RMS is used to show the effectiveness of the designed controller.



(a)



(b)



(c)

Fig. 11. The time response of the system under excitation of random road. (a) SD, (b) FSWS and (c) BVA

The damping control force generated by MR damper for front suspension in random road case is provided in Fig. 13. It can be concluded from Fig. 13, that the damper control force shows the similar variation trend for SMC and SMC-PID controlled system, which means that the MR damper can precisely track the desired control force. Furthermore, the comparison of the input control voltage for SMC and SMC-PID controlled system is shown in Fig. 14. The simulation results for this case to prove the validity of the modified Bouc-wen model of MR-damper.

The percentage reductions of RMS values of SD, FSWS and BVA are considered for comparative analysis as listed in Tables.5 (a-c). The RMS values of SD, FSWS and BVA for SMC-PID controlled suspension system are reduced by 23.26%, 21.13% and 30.70%, respectively when compared to SMC controlled suspension system. Similarly, the RMS values of SD, FSWS and BVA for SMC-PID controlled suspension system are reduced by 26.38%, 26.88% and 40.11%, respectively when compared to MR-Passive suspension system. The comparison indicated that the semi-active vehicle suspension system controlled using SMC-PID offers overall good effectiveness, which can provide the advanced suspension performance and improve ride comfort in general.

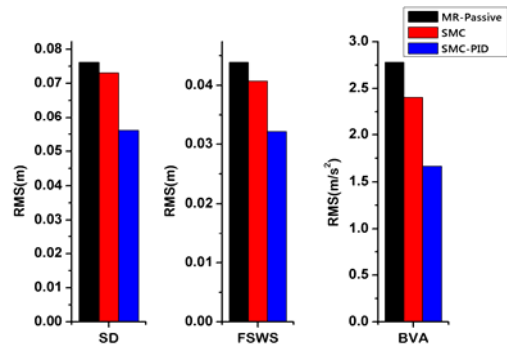


Fig. 12. The RMS values of SD, FSWS and BVA of the system under RI road.

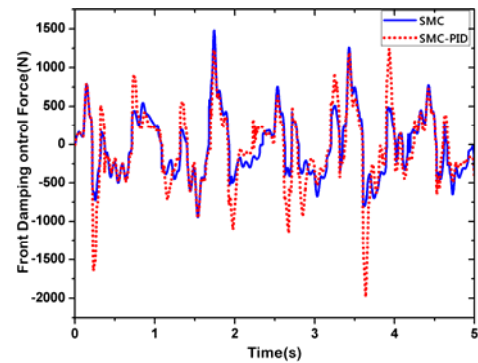


Fig. 13. The control force of front wheel for RI.

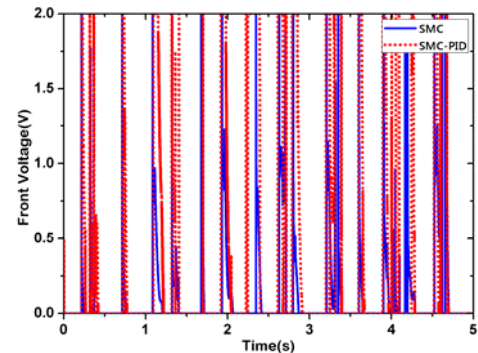


Fig. 14. Input control voltage for MR-damper.

Table 5(a). The RMS values of SD for RI

System Type	SD (m)	% Reduction Respect to MR-Passive	% Reduction Respect to SMC
MR-Passive	0.0762	---	---
SMC	0.0731	4.10	---
SMC-PID	0.0561	26.38	23.26

Table 5(b). The RMS values of SWS for RI

System Type	FSWS (m)	% Reduction Respect to MR-Passive	% Reduction Respect to SMC
MR-Passive	0.0439	---	---
SMC	0.0407	7.29	---
SMC-PID	0.0321	26.88	21.13

Table 5(c). The RMS values of BVA for RI

System Type	BVA (m/s ²)	% Reduction Respect to MR-Passive	% Reduction Respect to SMC
MR-Passive	2.7796	---	---
SMC	2.4024	13.57	---
SMC-PID	1.6648	40.11	30.70

5. CONCLUSIONS

The ride quality enhancement is the ambitious issue in the automobile industry. In this study, in order to improve the ride quality of vehicles, SMC with the PID sliding surface is designed as the system controller. For the damper controller the continuous state controller was applied. The particle swarm optimization (PSO) algorithm is used to be an effective searching technique for optimum PID sliding surface controller gains of semi-active MR damped vehicle suspension system. A dynamical model of a semi-active MR damped half-car model was derived and simulated. The HCM with MR-Passive, SMC and SMC-PID are simulated in time domain under bump and random road excitations using MATLAB/Simulink software. The performance of SMC-PID controlled suspension system is compared with SMC controlled and MR-Passive suspension system. The numerical and simulation results indicated that the root mean square and peak to peak values of SD, FSWS and BVA are the lowest in case of SMC-PID controller. Hence, the SMC-PID is capable to improve ride comfort over the MR-Passive and SMC.

The other SMC types such as Fuzzy SMC, terminal SMC and fractional order Fuzzy SMC can improve the performance further. The simulated controller has to be validated in real-time experimental setup.

ACKNOWLEDGEMENT

This research has been supported by Natural Science Foundation of China Government, Grant No (11472135) and Science Challenge Project, Grant No (JCKY2016212A506-0104). This support is thankfully acknowledged.

REFERENCES

- Bashir, A. O., Rui, X., Abbas, L. K. & Zhou, Q. (2018). MR-damped Vehicle Suspension Ride Comfort Enhancement Based on an intelligent Proportional-Integral-Differential Sliding Mode Control. *Journal of Control Engineering and Applied Informatics*, 20, 11-21.
- Batterbee, D. & Sims, N. (2007). Hardware-in-the-loop simulation of magnetorheological dampers for vehicle suspension systems. *Proceedings of the Institution of Mechanical Engineers, Part I: Journal of Systems and Control Engineering*, 221, 265-278.
- Chen, B.-C., Shui, Y.-H. & Hsieh, F.-C. (2011). Sliding-mode control for semi-active suspension with actuator dynamics. *Vehicle System Dynamics*, 49, 277-290.
- Choi, S.-B. & Kim, W.-K. (2000). Vibration control of a semi-active suspension featuring electrorheological fluid dampers. *Journal of Sound and vibration*, 3, 537-546.
- Choi, S., Choi, J., Lee, Y. & Han, M. (2003). Vibration control of an ER seat suspension for a commercial vehicle. *Journal of dynamic systems, measurement, and control*, 125, 60-68.
- Demir, O., Keskin, I. & Cetin, S. (2012). Modeling and control of a nonlinear half-vehicle suspension system: a hybrid fuzzy logic approach. *Nonlinear Dynamics*, 67, 2139-2151.
- Dyke, S., Spencer Jr, B., Sain, M. & Carlson, J. (1996). Modeling and control of magnetorheological dampers for seismic response reduction. *Smart materials and structures*, 5, 565.
- Eberhart, R. & Kennedy, J. A new optimizer using particle swarm theory. *Micro Machine and Human Science*, (1995). MHS'95., Proceedings of the Sixth International Symposium on, 1995. IEEE, 39-43.
- Edwards, C. & Spurgeon, S. (1998). *Sliding mode control: theory and applications*, Crc Press.
- Eker, I. (2006). Sliding mode control with PID sliding surface and experimental application to an electromechanical plant. *ISA transactions*, 45, 109-118.
- El-taweel, H. & Metered, H. (2018). Optimal lumped parameters estimation of vehicle passive suspension system using genetic algorithm. *Journal of Advances in Vehicle Engineering*, 5.
- Eltantawie, M. (2012). Decentralized neuro-fuzzy control for half car with semi-active suspension system. *International journal of automotive technology*, 13, 423-431.
- Ghazali, R., Sam, Y. M., Rahmat, M. F. A. & Hashim, A. W. I. M. (2011). Performance Comparison between Sliding Mode Control with PID Sliding Surface and PID Controller for an Electro-hydraulic Positioning System. *International Journal on Advanced Science, Engineering and Information Technology*, 1, 447-452.
- Hu, G., Liu, Q., Ding, R. & Li, G. (2017). Vibration control of semi-active suspension system with magnetorheological damper based on hyperbolic tangent model. *Advances in Mechanical Engineering*, 9, 1687814017694581.
- Karkoub, M. A. & Zribi, M. (2006). Active/semi-active suspension control using magnetorheological actuators. *International journal of systems science*, 37, 35-44.
- Kaya, I. (2007). Sliding-mode control of stable processes. *Industrial & engineering chemistry research*, 46, 571-578.
- Kelso, S. P. Experimental characterization of commercially practical magnetorheological fluid damper technology. *Smart Structures and Materials (2001): Industrial and Commercial Applications of Smart Structures Technologies*, 2001. International Society for Optics and Photonics, 292-300.
- Komurcugil, H. & Biricik, S. (2017). Time-varying and constant switching frequency-based sliding-mode control methods for transformerless DVR employing half-bridge VSI. *IEEE Transactions on Industrial Electronics*, 64, 2570-2579.
- Lai, C. Y. & Liao, W.-H. (2002). Vibration control of a suspension system via a magnetorheological fluid damper. *Modal Analysis*, 8, 527-547.
- Lam, A. H.-F. & Liao, W.-H. (2003). Semi-active control of automotive suspension systems with magneto-rheological

- dampers. *International Journal of Vehicle Design*, 33, 50-75.
- Metered, H., Bonello, P. & Oyadiji, S. (2010). An investigation into the use of neural networks for the semi-active control of a magnetorheologically damped vehicle suspension. *Proceedings of the Institution of Mechanical Engineers, Part D: Journal of Automobile Engineering*, 224, 829-848.
- Mu, X. Fuzzy neural sliding mode control based on genetic algorithm for multi-link robots. (2010) Chinese Control and Decision Conference, 2010. IEEE, 1766-1770.
- Paksoy, M., Guclu, R. & Cetin, S. (2014). Semiactive self-tuning fuzzy logic control of full vehicle model with MR damper. *Advances in Mechanical Engineering*, 6, 816813.
- PRrabakar, R., Sujatha, C. & Narayanan, S. (2009). Optimal semi-active preview control response of a half car vehicle model with magnetorheological damper. *Journal of sound and vibration*, 326, 400-420.
- Rajagopal, K. & Ponnusamy, L. (2014). Biogeography-based optimization of PID tuning parameters for the vibration control of active suspension system. *Journal of Control Engineering and Applied Informatics*, 16, 31-39.
- Rajkumar, B., Lakshmi, P. & Rajendiran, S. (2015). Vibration control of quarter car integrated seat suspension with driver model for different road profiles using fuzzy based sliding mode controller. *Advanced Computing (ICoAC)*, Seventh International Conference on, 2015. IEEE, 1-6.
- Rossi, C. & Lucente, G. (2004). H_∞ control of automotive semi-active suspensions. *Proceedings of the 1st IFAC Symposium on Advances in Automotive Control (AAC)*. Salerno, Italy.
- Spencer Jr, B., Dyke, S., Sain, M. & Carlson, J. (1997). Phenomenological model for magnetorheological dampers. *Journal of engineering mechanics*, 123, 230-238.
- Sung, K.-G. & Choi, S.-B. (2011). Design and control of a mr shock absorber for electronic control suspension. *Journal of the Korean Society for Precision Engineering*, 28, 31-39.
- Unger, A., Schimmack, F., Lohmann, B. & Schwarz, R. (2013). Application of LQ-based semi-active suspension control in a vehicle. *Control Engineering Practice*, 21, 1841-1850.
- Wang, D. & Liao, W. (2005). Semiactive controllers for magnetorheological fluid dampers. *Journal of Intelligent Material Systems and Structures*, 16, 983-993.
- Yao, J.-L., Shi, W.-K., Zheng, J.-Q. & Zhou, H.-P. (2013). Development of a sliding mode controller for semi-active vehicle suspensions. *Journal of Vibration and Control*, 19, 1152-1160.
- Yu, M., Dong, X., Choi, S. B. & Liao, C. (2009). Human simulated intelligent control of vehicle suspension system with MR dampers. *Journal of Sound and Vibration*, 319, 753-767.
- Yuvapriya, T., Lakshmi, P. & Rajendiran, S. (2018). Vibration suppression in full car active suspension system using fractional order sliding mode controller. *Journal of the Brazilian Society of Mechanical Sciences and Engineering*, 40, 217.
- Zhang, H., Wang, E., Zhang, N., Min, F., Subash, R. & Su, C. (2015). Semi-active sliding mode control of vehicle suspension with magneto-rheological damper. *Chinese Journal of Mechanical Engineering*, 28, 63-75.